Kono, Mitsuhiko; Baldwin, Kenneth G. H.; He, Yabai; White, Richard T.; Orr, Brian J..
CHAPS: a new precision laser-spectroscopic technique, *Journal of the Optical Society of America B-Optical Physics*, 2006; 23(6):1181-1189.

http://hdl.handle.net/2440/55640

CHAPS: a new precision laser-spectroscopic technique

Mitsuhiko Kono and Kenneth G. H. Baldwin

Research School of Physical Sciences and Engineering, Australian National University, Canberra, ACT 0200, Australia

Yabai He, Richard T. White,* and Brian J. Orr

Centre for Lasers and Applications, Macquarie University, Sydney, NSW 2109, Australia

We present a new technique for high-resolution pulsed spectroscopy that employs optical heterodyne detection to determine the instantaneous frequency of individual optical pulses, together with a frequency-binning method to generate high-precision spectra. We further demonstrate that active tuning of the light source is not necessary if the inherent frequency jitter of the source spans the spectral region of interest. This heterodyne-assisted approach to coherent pulsed spectroscopy (CHAPS) is applied in real time by using output from a pulsed, injection-seeded optical parametric oscillator–amplifier (OPO–OPA) system, the optical bandwidth of which is characterized via two-photon excitation of the $6S–8S$ transition in cesium. The resulting sub-Doppler measurements demonstrate the utility of CHAPS as a high-resolution spectroscopic technique and confirm that the pulsed OPO–OPA system operates very close to the Fourier-transform limit. © 2006 Optical Society of America

OCIS codes: 020.4180, 040.2840, 120.6200, 190.4970, 230.4320, 300.3700, 300.6320, 300.6410.

1. INTRODUCTION

The effective optical bandwidth of coherent radiation from pulsed sources used for precision spectroscopic measurements is limited principally by two factors. Firstly and fundamentally, the ultimate resolution is determined by the Fourier-transform (FT) limit imposed by the temporal profile of the optical pulse. Pulse-to-pulse variations of this temporal profile may also result in fluctuations in the FT-limited optical bandwidth. Secondly, the instantaneous optical frequency (obtained from the derivative of the phase of the optical electric field) may change during the pulse, further increasing the effective optical bandwidth. Such changes are often termed frequency "chirp." The instantaneous-frequency profile can also vary from pulse to pulse, adding to the uncertainty in spectroscopic measurements. Spectra measured using pulsed optical sources are usually accumulated over a large number of pulses to increase the signal-to-noise ratio, but these shot-to-shot variations often cause significant degradation of the spectroscopic resolution, relative to the single-shot optical bandwidth.

It has been known for some time that the instantaneous-frequency history of individual pulses of coherent light can be determined by optical heterodyne detection (OHD). Fee *et al.*[1] first demonstrated that, by overlapping a cw laser beam of very narrow optical bandwidth, (~ 1 MHz) with the beam from a pulsed laser, the resulting time-varying beat frequency can be detected on a fast photodiode. FT processing can then be used to reconstruct the temporal profile of the laser pulse as well as the instantaneous-frequency history. OHD has been further developed, for example, to characterize frequency chirp in either pulsed dye amplification of cw radiation[2–5] or in the signal output of an injection-seeded parametric oscillator–amplifier (OPO–OPA) system.[6–10] In both cases, a portion of the cw seed laser beam is split and frequency shifted to provide the reference beam for the OHD beat measurement. OHD characterization of frequency chirp has also been applied to precision measurement, such as determining the Lamb shift in the ground state of helium,[11–15] where an averaged value for the frequency chirp was used to correct the measured transition frequency.

To reduce the shot-to-shot degradation of spectra accumulated over many pulses, we have introduced a new technique[10] that we name coherent heterodyne-assisted pulsed spectroscopy (CHAPS). This method exploits OHD measurement for every pulse to determine a characteristic frequency for the pulse around which the instantaneous frequency varies. For this purpose we use the central beat frequency ν_b, which we define as the peak of the power spectrum of the beat waveform.[7] By binning the measured signal obtained from each pulse according to its characteristic frequency (e.g., ν_b), we can generate a more finely resolved spectrum and virtually eliminate inhomogeneous broadening due to frequency jitter of the optical source. This CHAPS approach is thereby able to substantially improve the effective spectroscopic resolution of a pulsed coherent light source, in particular an injection-seeded laser or OPO–OPA system. Moreover, inherent frequency jitter in the optical source can in some circumstances[10] be turned to an advantage by providing a range of characteristic frequencies that span the spectral feature(s) to be measured, thereby obviating the need to
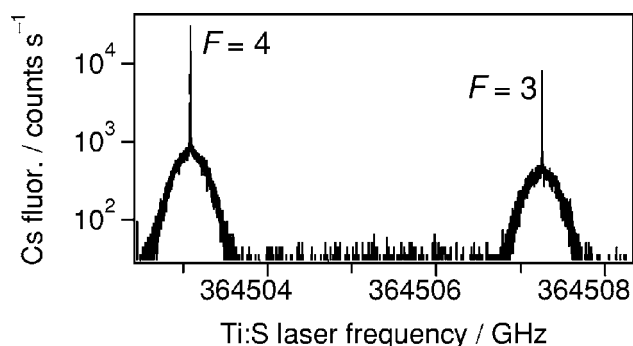
Fig. 1.   Logarithm of the cw Cs TPE fluorescence signal as a function of Ti:S laser frequency, showing the $F=3$ and $F=4$ hyperfine components of the $6S-8S$ transition.

actively scan the optical frequency of the light source. For example, this enables a cw injection-seeding laser to be precisely locked to a known, fixed frequency to which the characteristic frequency of each pulse can then be referenced. Furthermore, because the instantaneous-frequency history of each pulse is recorded, those pulses for which the frequency chirp is measured to be unacceptably high can be rejected, in order to further improve the spectroscopic resolution.

This paper presents the results of a detailed application of CHAPS to characterize the optical bandwidth of coherent light from an injection-seeded pulsed OPO–OPA system. As a spectroscopic test bed we have used the well-established $6S-8S$ two-photon transition in atomic cesium;[16,17] this has a very narrow (<1 MHz) natural linewidth, significantly less than the optical bandwidth of the light from the pulsed OPO–OPA source whose FT-limited value is at least 18 MHz. We are also able to correlate the derived spectra with the chirp characteristics of individual pulses, to show that pulse selection can be used to enhance the spectroscopic resolution of the measurement.

2. INSTRUMENTATION

The OPO system has been described in detail previously,[8–10] so only a brief outline will be presented here. A periodically poled KTiOPO$_4$ crystal (PPKTP) in a bow-tie cavity is injection seeded using a titanium–sapphire ring laser (Ti:S laser; Coherent 899) pumped by an Ar$^+$ laser (Coherent Innova 300). The OPO cavity is locked to the frequency of the single-longitudinal-mode (SLM) Ti:S laser output, which has an optical bandwidth of <1 MHz. The PPKTP OPO crystal is pumped by the 532 nm SLM output of a frequency-doubled Nd:YAG laser (Continuum Powerlite 8000) that has been custom built to provide a longer-than-usual FWHM pulse duration of ~27 ns in order to decrease the FT-limited optical bandwidth. Typically the OPO is pumped at 532 nm by ~20 μJ pulses (~2.5 times the free-running threshold) and yields a total of ~4.5 μJ/pulse of SLM output at the OPO signal wavelength (~822 nm in this work). When the wavelength of the Ti:S injection-seeding laser is set to the peak of the (temperature-tuned) OPO gain curve, OHD measurements demonstrate that the frequency chirp of the OPO signal output is close to zero. The chirp can be made

either positive or negative by respectively increasing or decreasing the separation of the seed-laser wavelength from the OPO gain peak.[6,8]

An OPA stage has been added to the OPO system in order to increase the output power and to determine the effect of optical parametric amplification on the chirp characteristics of the signal output pulse. The OPA uses a LiNbO$_3$ crystal (with birefringent noncritical $\theta=90°$ type I phase matching) mounted in a temperature-controlled housing. For the purposes of these experiments, the OPA stage was operated under three distinct conditions: at zero OPA pump power (i.e., OPO only), at full OPA pump power (designated "OPA") with 40 mJ of 532 nm pump radiation, or at half OPA pump power (subsequently designated "OPA/2"). Corresponding signal pulse energies measured after the OPA stage are ~1.5, ~6.0, and ~2.7 μJ, respectively, noting that the OPO output pulse energy is considerably attenuated during transmission through the beam-transfer optics and the unpumped OPA crystal. Energy gain factors up to ~8 can be achieved with this long-pulse system, using OPA pump energies up to ~40 mJ.[18]

The Ti:S laser can generate up to 1 W of power at the wavelength of 822.47 nm that is required for Cs $6S-8S$ two-photon excitation (TPE). This was sufficient to enable the Ti:S laser output to be split (after appropriate attenuation) into three separate beams for the following purposes: one beam (~10 mW) injection seeding the OPO cavity (as outlined above); a second beam (~2 mW) providing the cw reference frequency for OHD purposes; and a third beam (~200 mW) enabling cw TPE measurements of Cs vapor and simultaneous frequency monitoring by a wavemeter (Burleigh WA-1100) and a Fabry–Perot interferometer.

The second Ti:S laser beam is frequency shifted by ~720 MHz using an acousto-optic modulator (AOM) and combined collinearly with the signal beam from the pulsed OPO–OPA system; the combined beams are then focused onto a fast photodetector (New Focus 1623; rise time 1 ns) to generate the OHD beat signal.[8] The stability of the AOM radio-frequency driver was measured to be better than ±0.1 MHz/h after 3 h of warm-up operation.

The third Ti:S laser beam was used to make cw TPE measurements in an optical cell containing Cs vapor maintained at a temperature of ~90 °C. This beam (diameter ~1 mm) was retroreflected without focusing through the Cs cell, counterpropagating with a parallel-
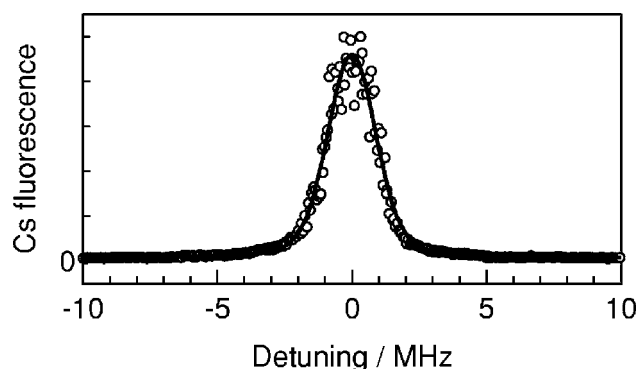

Fig. 2.   Sub-Doppler $F=3$ peak in the $6S-8S$ cw TPE spectrum of Cs vapor, with a Voigt-profile fit (2.2 MHz FWHM).
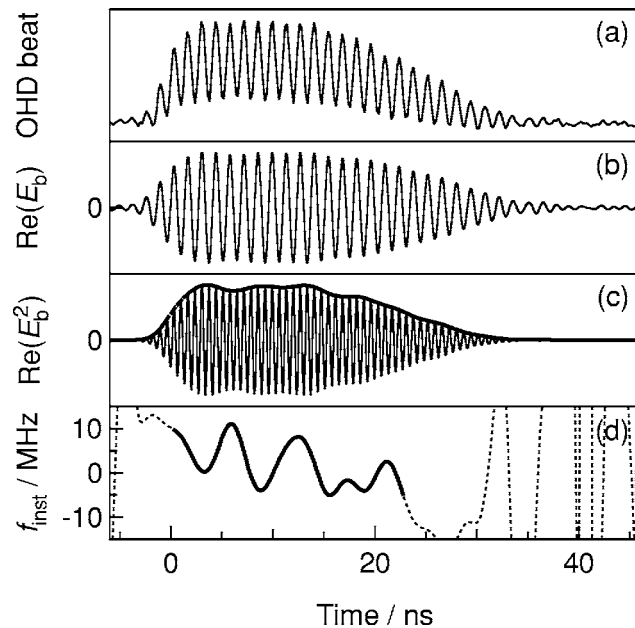
Fig. 3. (a) Typical OHD beat waveform for a negatively chirped OPO pulse. (b) Reconstructed beat component E_b (real part only) derived by the FT method. (c) Real part of $E_b{}^2$, with its envelope $E_0{}^2$ as a solid curve. (d) Instantaneous frequency f_{inst} derived from E_b by the FT method, with the solid curve indicating the FWHM region of the reconstructed pulse profile, wherein the total chirp (linear fit) is -9.1 ± 1.3 MHz.

ism of $\leqslant 2$ mrad (causing the TPE peak to have residual Doppler broadening of less than 1 MHz FWHM). The cw TPE spectrum was measured by detecting the spontaneous fluorescence cascade at ~ 460 nm from the $7P-6S$ transition using a bandpass filter (Corning 4-76) and a photomultiplier (Thorn EMI 9813B) operating in photon-counting mode.

A similar fluorescence-detection arrangement was used to measure pulsed TPE spectra in a second Cs vapor cell, with a photomultiplier (Hamamatsu 1P-28 with Stanford Research Systems SR445 preamplifier, combined rise time ~ 2.5 ns) in current-mode configuration, to process the higher fluorescence signal excited by the high-peak-power signal radiation from the pulsed OPO–OPA. For all the pulsed TPE experiments, the frequency of the cw Ti:S laser used to seed the OPO was manually locked to the peak of the $F=4$ component of the cw TPE spectrum and was kept above $\sim 70\%$ of the maximum cw TPE signal amplitude at all times.

3. CW TPE LINEWIDTH MEASUREMENTS

An example of a cw TPE spectrum, with the Ti:S laser scanned across the $F=3$ and $F=4$ hyperfine components of the Cs $6S-8S$ transition,[16,17] is shown in Fig. 1. The Doppler-broadened pedestal for each transition underlies a much narrower peak, corresponding to the sub-Doppler signal. A Gaussian fit to the pedestals with a common width yields a FWHM of 427.8 MHz on the Ti:S laser frequency scale, consistent with a Cs sample temperature of 84 °C.

A higher-resolution scan of the $F=3$ peak is shown in Fig. 2, together with a Voigt-profile fit to the data points.

The best fit has Gaussian and Lorentzian components of 1.81 ± 0.09 MHz FWHM and 0.56 ± 0.12 MHz FWHM, respectively; comparable results are obtained for the $F=4$ peak. Transit-time broadening is estimated to contribute ~ 0.04 MHz, which is insignificant compared with the 0.75-MHz natural linewidth of the transition.[17] Our high-resolution cw spectroscopic measurements of the Cs $6S-8S$ transition are consistent with previous studies.[16,17,19] The combined cw TPE linewidth of ~ 2.2 MHz FWHM on the Ti:S laser frequency scale includes contributions from laser instrumentation and from beam alignment but is much smaller than the FT limit of the pulsed OPO–OPA output that is of principal concern to us in this paper. Moreover, since the frequency of the Ti:S laser was manually locked within $\sim 70\%$ of the maximum cw TPE signal amplitude while injection seeding the OPO, this indicates that the frequency of the Ti:S injection seeder is maintained within <1 MHz of the TPE peak.

4. OHD ANALYSIS

The algorithm for analyzing the pulsed-beat signals has been presented in detail elsewhere[7] and will be described briefly here in the context of the OHD experiments used for pulse-by-pulse diagnosis of the instantaneous-frequency characteristics of the OPO–OPA signal output. A typical OHD beat waveform is shown in Fig. 3(a), which is then FT processed and filtered to select the positive-frequency sideband centered around the AOM frequency (~ 723 MHz). The data are then backtransformed into the time domain to yield the reconstructed OHD beat component E_b. The real part of E_b and of $E_b{}^2$ is shown in Figs. 3(b) and 3(c), respectively.

The reconstructed pulse power profile is given by the envelope $E_0{}^2$ of the squared reconstructed beat component $E_b{}^2$, shown as a dashed curve in Fig. 3(c). When the reconstructed power profiles are compared with power profiles measured directly, analysis indicates a 1σ standard deviation of $\sim 10\%$ over the whole profile, with the measured profile FWHM duration being $\sim 4\%$ longer than that of the reconstructed power profile. The corresponding difference between the FT-limited optical bandwidths of measured and reconstructed pulses is around -3%.
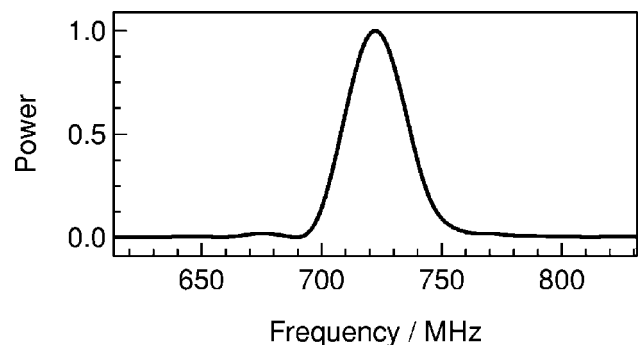

Fig. 4. FT power spectrum (29.2 MHz FWHM) of the negatively chirped reconstructed beat component E_b shown in Fig. 3(b). The central beat frequency ($\nu_b = 722.3$ MHz) corresponds to the peak of the FT power spectrum (normalized to 1.0).
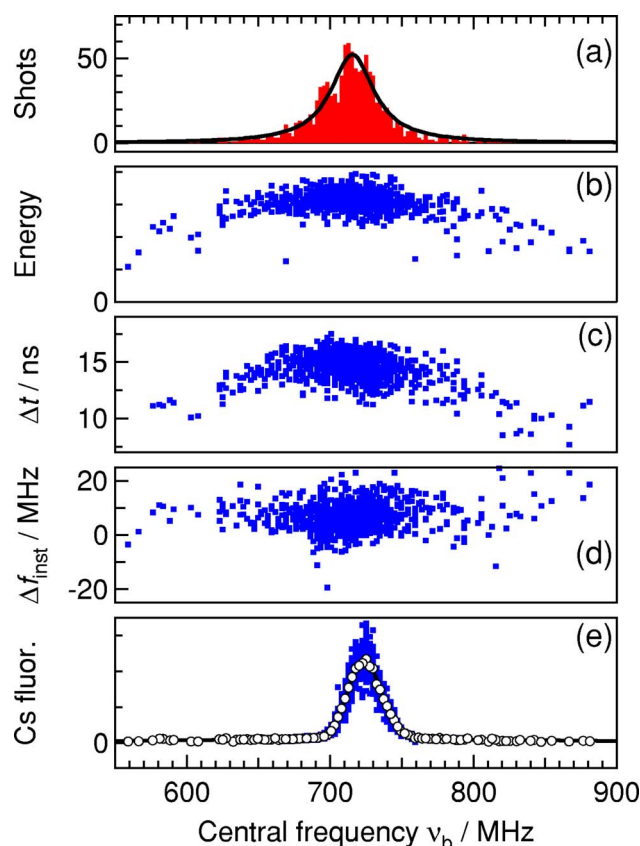
Fig. 5.   (Color online) Central-frequency binned data (1104 shots) for a full OPA with positive chirp. (a) Histogram of the number of pulses, with a Lorentzian fit (solid curve, 50 MHz 1σ width) and average central beat frequency 715 MHz. (b) OPA pulse energies (arbitrary units). (c) FWHM duration Δt of the temporal power profile, with an average of 14.2 ± 2.2 ns. (d) Total chirp (linear fit) over the FWHM region, with an average chirp of 7.0 ± 7.0 MHz. (e) Cs TPE fluorescence spectrum, showing binned individual pulse values (filled circles), the average value for each bin (open circles), and a two-component Gaussian fit (solid curve). The FWHM linewidth $\Delta\nu_b$ and fitting error for the sub-Doppler peak are equal to 27.4 ± 0.4 MHz.

Temporal variations of the instantaneous frequency f_{inst}, obtained from the corresponding backtransformation, are displayed in Fig. 3(d), with the region between the FWHM power limits highlighted. The total frequency chirp, defined by a linear fit[6–8] to this region, is negative in the instance shown (-9.1 ± 1.3 MHz) and has some oscillatory structure.

The instantaneous-frequency history is derived from the OHD measurement, which is also used to characterize the spectroscopic information obtained for each pulse. We start with an OHD beat waveform that is acquired during a 100 ns period using a 5 gigasample s^{-1} oscilloscope (i.e., spanning 500 sample points). The data set is extended by zero padding to 2048 data points before taking the FT, which yields a bin width in the frequency domain of 2.44 MHz. A typical FT power spectrum, corresponding to the reconstructed beat component E_b depicted in Fig. 3(b), is shown in Fig. 4 under negatively chirped operating conditions.

The key piece of information derived from the OHD procedure is the central beat frequency ν_b, which we define as the frequency bin that contains the peak of the FT power spectrum near the AOM frequency. For each OPO–OPA output pulse, ν_b is used as a characteristic frequency; it is the point around which the instantaneous frequency varies (chirps).

5. CHAPS TECHNIQUE

The CHAPS technique[10] enables us to display spectroscopic information as a function of the value of ν_b obtained for each pulse using the OHD method. This approach is illustrated in Figs. 5 and 6, where spectroscopic data associated with each full-power OPA pulse are binned according to the value of ν_b for that pulse. Figure 5 and 6 refer, respectively, to positive and negative chirp; zero-chirp results comparable with panels (a), (d), and (e) have been reported in a previous paper.[10]

The top panel (a) in each figure shows the distribution of the number of shots with the indicated central frequencies; this forms a histogram with an approximately Lorentzian profile (solid curves), composed of 2.44 MHz wide frequency bins. Note that the injection-seeding laser frequency is locked at all times within 1 MHz of the peak of the cw TPE resonance, so the 1σ width of the central-frequency distribution (~50 MHz) is due almost entirely to the frequency jitter inherent in the signal output from the OPO–OPA system. Likely sources of frequency jitter

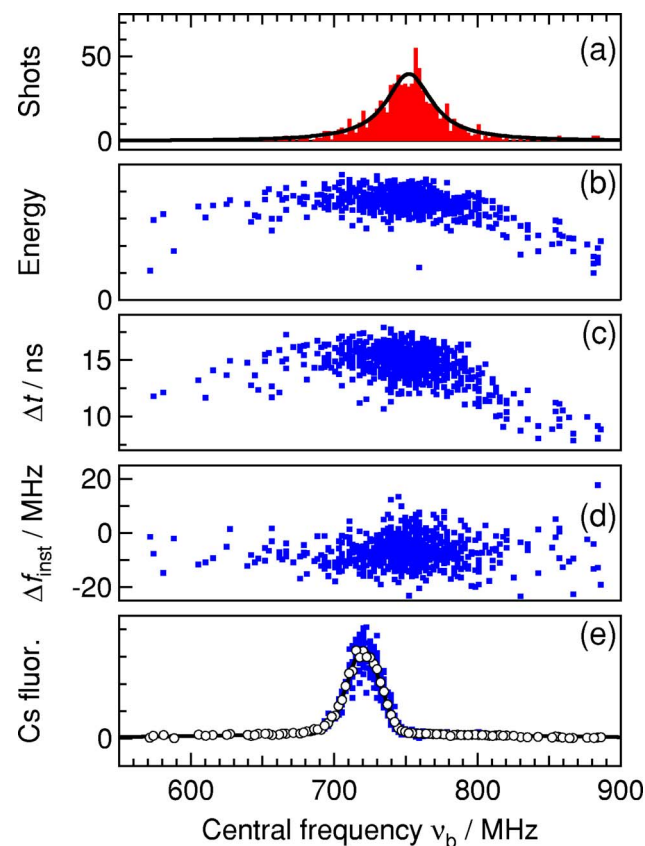Fig. 6.   (Color online) As for Fig. 5, but with a negative chirp (878 shots). (a) Histogram with a Lorentzian fit and an average central beat frequency 751 ± 47 MHz. (b) OPA pulse energies. (c) FWHM Δt with an average of 14.5 ± 2.1 ns. (d) Total chirp, with an average of -6.9 ± 7.6 MHz. (e) Cs TPE fluorescence spectrum with FWHM linewidth $\Delta\nu_b$ for the sub-Doppler peak equal to 27.1 ± 0.3 MHz.
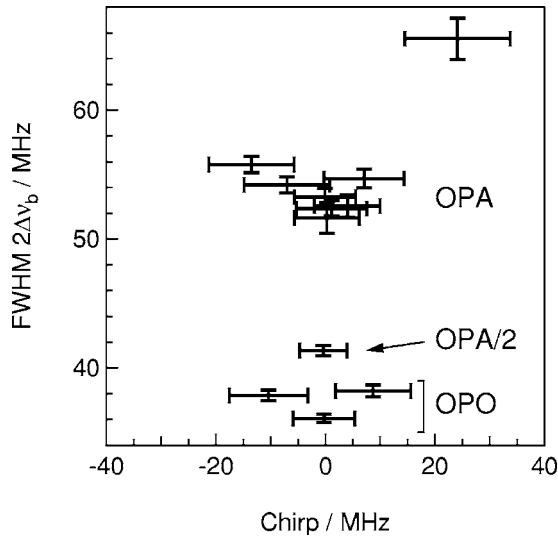
Fig. 7.   Fluorescence-detected Cs TPE FWHM linewidth $2\Delta\nu_b$ plotted against the average of the total chirp over the FWHM temporal profile. Horizontal and vertical error bars indicate the 1σ standard deviation of the chirp, and the fitting error of $2\Delta\nu_b$, respectively.

include mechanical and acoustical vibrations, causing small variations in the OPO cavity length. It is also noticeable that negatively (or positively) chirped pulses yield a shift in the frequency histogram to higher (or lower) central frequencies. This may be due to frequency pulling of the OPO signal output toward the OPO gain peak, since detuning the seed laser to frequencies higher (lower) than the OPO gain peak creates negatively (positively) chirped pulses.[6]

Panels (b) and (c) in Figs. 5 and 6 show the dependence on ν_b of the pulse energy (measured by integrating the beat waveform), and the FWHM duration Δt of the reconstructed temporal power profile. Both show a slightly peaked distribution near the most probable value of ν_b; this contrasts with the chirp data shown in panel (d), for which the distribution is almost flat. The invariance of chirp with ν_b is important spectroscopically, because it yields an average chirp over all shots of $+7.0\pm7.0$ MHz or -6.9 ± 7.6 MHz from Figs. 5 and 6, respectively (all quoted uncertainties are 1σ standard deviations unless otherwise noted).

Likewise, a plot of the Cs TPE fluorescence signal versus ν_b yields the TPE spectra in Figs. 5(e) and 6(e), which indicate individually binned pulse values (filled circles) and their average for each bin (open circles). A two-component Gaussian function with a common peak frequency is fitted to the averaged data to represent the sub-Doppler peak and the underlying pedestal. Note that, on the Ti:S laser frequency scale, the FWHM linewidth $\Delta\nu_b$ for the sub-Doppler peak is similar ($\sim$27 MHz) for the two data sets, which have almost identical chirp magnitudes but opposite sign. This is a central result of this paper; by use of the CHAPS technique, a sub-Doppler atomic linewidth ($\sim$27 MHz FWHM) has been resolved using OPO radiation that itself has a considerably greater pulse-to-pulse frequency jitter ($>$40 MHz FWHM), and this has been achieved without the need to actively scan the optical frequency.

6. PULSED TPE LINEWIDTH ANALYSIS

Figure 7 displays values of the Cs TPE FWHM linewidth $2\Delta\nu_b$ (where the factor of 2 accounts for the two-photon process) for the various OPO–OPA configurations, as a function of the average total frequency chirp. The chirp is associated primarily with the phase mismatch due to displacement of the seed laser wavelength from the center of the OPO gain profile.[8] Results for the various OPO and OPA power settings indicate that the narrowest linewidths correspond to the lowest chirp settings, as expected.

The Cs TPE FWHM linewidth $2\Delta\nu_b$ increases as a function of the pulse duration, which decreases with amplification. The OPA gain tends to be concentrated in the central, highest-power region of output pulses, so increased amplification reduces the FWHM duration of the pulses[18] and hence increases their FT-limited optical bandwidth. This effect is shown in Fig. 8 under zero-chirp conditions. The lower abscissa in Fig. 8 is the FWHM pulse duration Δt for different amplification settings, whereas the upper abscissa shows corresponding OPO–OPA signal pulse energies. There is a clear correspondence between increasing OPO–OPA power and decreasing pulse duration,[18] which in turn increases the FT-limited Cs TPE linewidth $2\Delta\nu_b$ (as shown in Fig. 7).

The various contributions to the Cs TPE linewidth $2\Delta\nu_b$ can be understood by comparing the FT power spectrum of the OHD beat waveform (containing the variations in instantaneous frequency) with the optical bandwidth to be expected purely from the FT limit imposed by the temporal profile of the pulse. As expected for a two-photon process, there is an approximately quadratic power dependence of the Cs TPE signal amplitude on the OPO–OPA pulse power.

To reflect the nonlinear-optical polarization of the Cs atoms via two-photon excitation, we calculate the FT power spectrum for the square of the reconstructed beat component, $E_b{}^2$. An example is presented in Fig. 9 (solid curve), which shows the FT power spectrum of the square of the beat component $E_b{}^2$ from Fig. 3(c). This is in contrast to the FT of the reconstructed beat component E_b shown in Fig. 4; the corresponding frequency scale (top abscissa in Fig. 9) is twice that of the Ti:S laser frequency
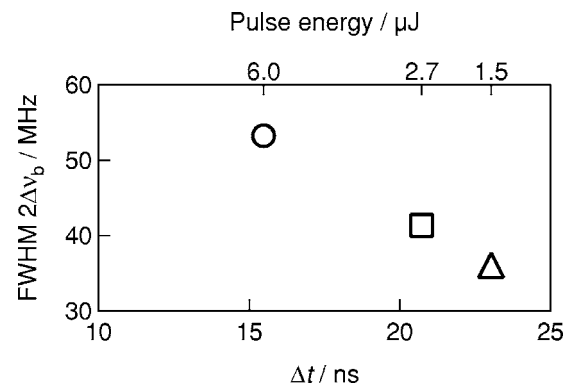

Fig. 8.   Cs TPE FWHM linewidth $2\Delta\nu_b$ for zero-chirp OPO–OPA operating conditions plotted against the averaged OPO–OPA pulse duration Δt (lower abscissa). Triangle, OPO only; square, OPA/2; circle, full OPA. The upper abscissa shows the corresponding signal-pulse energies.
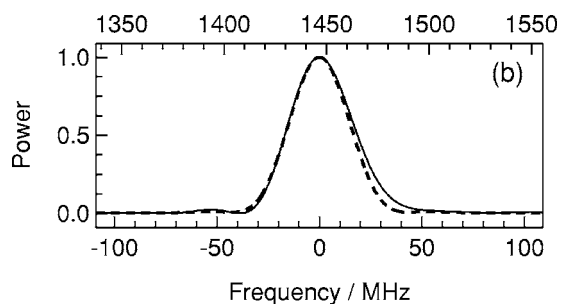
Fig. 9. FT power spectra for the negatively chirped data shown in Fig. 3 (normalized to 1.0). The solid curve is for the squared reconstructed beat component E_b^2 as in Fig. 3(c) (35.5 MHz FWHM, upper abscissa). The dashed curve is for the reconstructed pulse power temporal profile E_0^2 (33.5 MHz FWHM, lower abscissa, taking the central TPE beat frequency $2\nu_b$ as origin).

scale shown in Fig. 4. Note that the solid curve in Fig. 9 is asymmetric, which reflects the contribution to the power spectrum due to variations in instantaneous frequency. As expected, it is also broader (35.5 MHz FWHM) than the symmetric FT-limited power spectrum (dashed curve in Fig. 9) calculated from the temporal profile E_0^2 of the reconstructed pulse power (33.5 MHz FWHM). Both the asymmetry and the larger bandwidth of the solid-line power spectrum are thus attributable to the presence of variations in the instantaneous frequency that give rise to frequency chirp.

We now use this information to determine how closely the TPE linewidths correspond to the FT-limited bandwidth expected from the power temporal profile. In Fig. 10 we plot the measured Cs TPE FWHM linewidth $2\Delta\nu_b$ versus the FWHM spread of the average of the power spectra calculated by two methods. The first (filled symbols) calculates the FT limit imposed by the pulse temporal profile by taking the FT of the reconstructed pulse power temporal profiles E_0^2 (e.g., the dashed curve in Fig. 9). The second (open symbols) calculates the slightly broader FT power spectrum that is expected to correspond to the combined contributions of the temporal profile and the instantaneous frequency. This is calculated by taking the FT of the squared reconstructed beat components E_b^2 (corresponding to the solid curve in Fig. 9).

The pairwise proximity of filled and open symbols plotted in Fig. 10 shows that the OPO–OPA system operates very close to the FT limit, particularly for the zero-chirp settings indicated by the arrows. As the chirp increases, there is a trend away from the FT limit (i.e., the pairs of filled and open data points become more widely separated). Furthermore, the measured TPE linewidth is somewhat larger than that expected, for example, for coherent light with a pure Gaussian spectrum,[20] as indicated by the dashed line (with unity slope through the origin) shown in Fig. 10. This difference may reflect complexities in the relationship between the two- and single-photon bandwidths that depend on the characteristic coherence of the radiation fields involved.[20–22] For instance, there is recent evidence[22] that narrow two-photon resonances can be obtained through coherently controlled absorption of a broadband optical field, comprising a distribution of correlated pairs of narrowband components.

Pulse-by-pulse OHD characterization of OPO–OPA signal output enables selection of individual pulses with narrower optical bandwidth, thereby yielding a substantial improvement in spectroscopic resolution. To assist this selection process, we employ three-dimensional maps of the distribution of binned pulse properties such as chirp or pulse duration (plotted on the ordinate) against ν_b (plotted on the abscissa), with average fluorescence intensities represented by the depth of shading. To illustrate this for the zero-chirp case, Fig. 11(a) shows such a three-dimensional portrayal of the fluorescence intensity as a function of ν_b for $\sim10^3$ OPA pulses of varying FWHM pulse duration Δt. (Note that the spectra contain no information on the number of pulses with these characteristics.) As expected near the FT limit, the linewidth $\Delta\nu_b$ becomes narrower as Δt increases. To illustrate this aspect, Fig. 11(b) depicts the binned Cs TPE fluorescence intensity data points with $\Delta t > 16$ ns (26% of all data), for which a Gaussian fit is shown. The FWHM linewidth $\Delta\nu_b$ (26.1 ± 0.4 MHz) is less than that averaged over all data (26.6 ± 0.3 MHz), and marginally less than that for 59% of all data averaged with $\Delta t > 15$ ns (26.2 ± 0.3 MHz). The value of $\Delta\nu_b$ decreases further for the 4% of results with $\Delta t > 17$ ns (25.5 ± 1.1 MHz). It is clear that narrower linewidths $\Delta\nu_b$ associated with longer Δt can be traded off against the size of the statistical base, although the latter may be somewhat offset since longer pulse durations also yield higher fluorescence signals (lighter regions) that have a better signal-to-noise ratio.

A similar three-dimensional plot under the same conditions (full OPA, zero average chirp) shows the spectroscopic distribution as a function of individual pulse frequency chirp in Fig. 12. The spectra appear to be narrower in the chirp range between ±10 MHz, although only 6% of the data lie outside this region. Aggregation of data [in a fashion similar to that displayed in Fig. 11(b)]
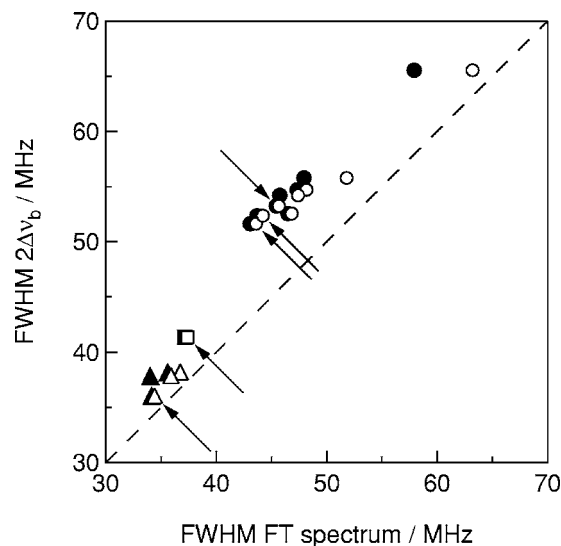

Fig. 10. FWHM linewidth $2\Delta\nu_b$ of Cs TPE fluorescence plotted against the FWHM of the average of FT power spectra calculated from the reconstructed pulse-power temporal profile E_0^2 (filled symbols) and from the square of the reconstructed beat component E_b^2 (open symbols). Triangles, OPO only; square, OPA/2; circles, full OPA. Zero-chirp OPO–OPA settings are marked with arrows.
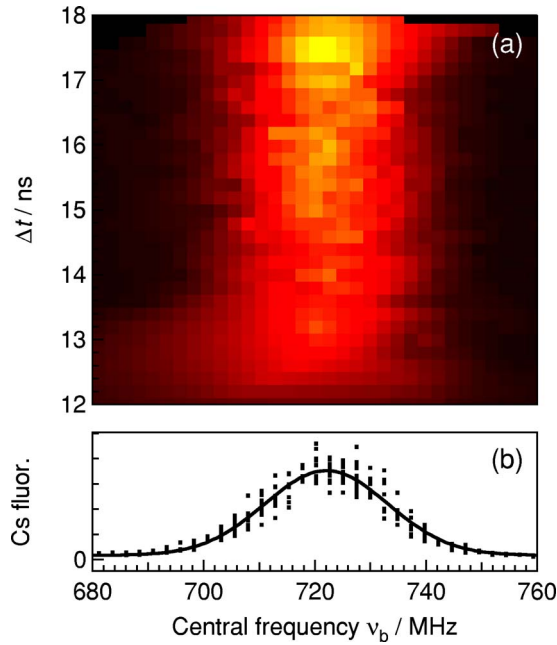
Fig. 11. (Color online) Full OPA with zero chirp (1023 shots). (a) Three-dimensional plot of the average peak TPE fluorescence spectra showing the signal level (lightest shades, highest intensity; darkest shades, lowest intensity) at the indicated central beat frequency ν_b, as a function of pulse FWHM Δt (units of 0.2 ns, vertical axis); (b) Spectrum showing individual data point fluorescence values for $\Delta t > 16$ ns. Solid curve is a Gaussian fit (FWHM 26.1 ± 0.4 MHz).

around the zero-chirp range (± 1 MHz) that contains 19% of data, yields a Gaussian spectrum with FWHM linewidth $\Delta\nu_b$ of 25.8 ± 0.5 MHz. This can be compared with 26.4 ± 0.3 MHz, aggregated over ± 3 MHz (54%), and with 26.6 ± 0.3 MHz, aggregated over all data. Hence data selection around the zero-chirp region can further improve the spectroscopic resolution. Likewise, analysis of data that are positively or negatively chirped also indicates that spectroscopic resolution can be improved by pulse selection, even though the OPO signal output has a substantially larger spectroscopic bandwidth.

Finally, the CHAPS technique is able to detect a slight difference between TPE spectra plotted using either the central beat frequency ν_b or the mean beat frequency $\bar{\nu}_b$ (e.g., as determined from the FT power spectrum shown in Fig. 4). Figure 13 shows the peak positions of the Cs TPE spectra, referred to (a) ν_b and (b) $\bar{\nu}_b$, plotted as a function of $\langle \nu_b - \bar{\nu}_b \rangle$; this frequency difference is averaged over all data for each chirp and OPA setting.

Figure 13 shows that, for zero-chirp settings, ν_b and $\bar{\nu}_b$ yield almost identical TPE peak values. For negative chirp, the chirp-induced asymmetry (e.g., as in Fig. 4) causes the mean ($\bar{\nu}_b$) to shift to higher frequencies, which in turn shifts the TPE peak position to lower frequencies, and vice versa for positive chirp. Consequently, Fig. 13(a) reveals a linear relationship between the TPE peak position and $\langle \nu_b - \bar{\nu}_b \rangle$. This suggests that, for nonzero-chirp values, the mean beat frequency $\bar{\nu}_b$ may be more appropriate than ν_b itself for characterizing the CHAPS data, as illustrated in Fig. 13(b). Apart from the right-most data point (for the largest positive chirp value of 55 MHz), the data show only a slight variation (± 1 MHz) with $\langle \nu_b$

$- \bar{\nu}_b \rangle$. (The 55 MHz chirp data point is also an outlier in Figs 7 and 10—top right-most point in each—and has a poor statistical overlap between the pulse histogram and the TPE peak position.) Nevertheless, there is a slight negative slope for data plotted using $\bar{\nu}_b$ in Fig. 13(b), although it is smaller in magnitude than the slope for data plotted using ν_b in Fig. 13(a).

7. CONCLUSIONS

We have demonstrated the use of a new pulsed spectroscopic technique, CHAPS,[10] that uses OHD to yield the characteristic frequency, the instantaneous frequency (including frequency chirp), and the temporal history of every pulse in real time. Either the central (i.e., peak) frequency ν_b or the mean frequency $\bar{\nu}_b$ of the FT power spectrum can be used to characterize the CHAPS data. Our results indicate that $\bar{\nu}_b$ may be more appropriate, particularly for pulses with large chirp. This characteristic frequency can then be used to establish the frequency scale for high-resolution spectroscopic measurements of interest. Such an approach effectively suppresses frequency jitter, which would otherwise inhomogeneously broaden the spectrum.

A central result of this paper is that the inherent frequency jitter of the pulsed coherent light source can be turned to substantial advantage by using CHAPS to create a spectrum without actively tuning the light source itself[10] [as demonstrated in Figs. 5(e) and 6(e)]. If the inherent frequency jitter does not span the spectral region of interest, then a second cw tunable laser can be locked to a known reference frequency while the injection-seeding laser for the pulsed coherent light source is scanned through the spectrum at well-controlled offset frequencies. The beat frequency between the two cw tunable lasers (reference and seed) can then be used to calibrate the spectrum absolutely, while the beat signal between radiation from either of the two cw tunable lasers and from the pulsed coherent light source can be used for the CHAPS measurement.
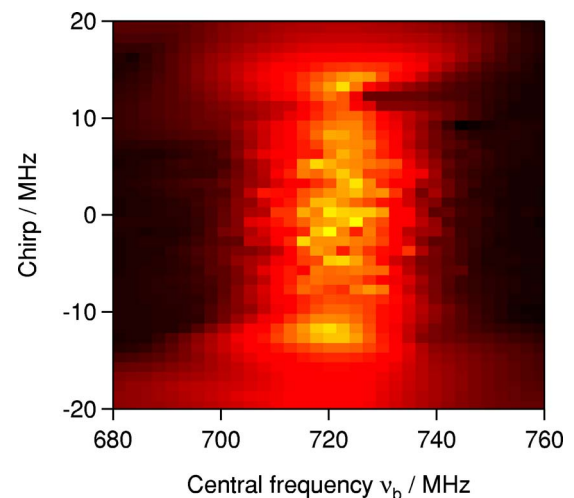

Fig. 12. (Color online) As for Fig. 11(a) (full OPA, zero chirp) except that the ordinate is now the total chirp over the FWHM temporal profile. The average chirp is -0.1 ± 5.5 MHz.
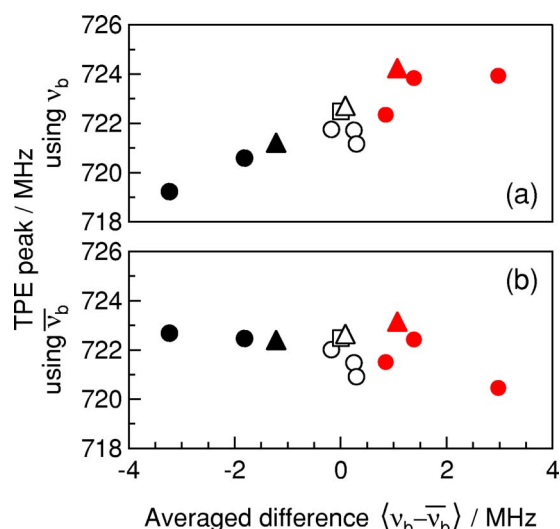
Fig. 13. (Color online) Peak position of the Cs TPE fluorescence measured using (a) the central (peak) beat frequency ν_b and (b) the mean beat frequency $\bar{\nu}_b$, plotted against the averaged frequency difference $\langle \nu_b - \bar{\nu}_b \rangle$. Triangles, OPO only; square, OPA/2; circles, full OPA. Left-most filled symbols, negative chirp; open symbols, zero chirp; right-most filled symbols, positive chirp.

We have used the CHAPS technique for real-time characterization of the output of a very narrowband SLM OPO–OPA system[6–9] using a sub-Doppler two-photon measurement of the $6S$–$8S$ transition in Cs.[10,16,17] The CHAPS data show that the OPO–OPA system operates very close to the FT limit, particularly when the frequency chirp in the signal output is set to zero. High-resolution, fluorescence-detected TPE spectra close to the FT limit were obtained by the CHAPS technique without needing to actively tune either the cw injection-seeding laser or the OPO itself. These pulsed TPE spectra have a sub-Doppler linewidth ($\sim$27 MHz FWHM) that is much narrower, by almost a factor of two, than the pulse-to-pulse frequency jitter ($>$40 MHz FWHM) of the unscanned OPO signal output itself. The ultimate accuracy of such spectroscopic measurements is $<$1 MHz, determined primarily by the calibration and stability of the cw Ti:S laser employed to injection seed the pulsed OPO system and to provide an OHD reference frequency. OHD-based pulse selection procedures (Figs. 11 and 12) have been used to further enhance the spectroscopic resolution by eliminating OPO–OPA shots that yield broader spectra. We anticipate that the CHAPS technique will find applications in precision pulsed spectroscopic measurements, such as the determination of the Lamb shift in helium,[11–15] where high-resolution pulsed light sources require extremely precise characterization and control.

ACKNOWLEDGMENTS

K. G. H. Baldwin's e-mail address is Kenneth.Baldwin@anu.edu.au.

*Present address, Industrial Research Ltd., P.O. Box 31-310, Lower Hutt, New Zealand.

REFERENCES

1. M. S. Fee, K. Danzmann, and S. Chu, "Optical heterodyne measurement of pulsed lasers: toward high-precision pulsed spectroscopy," Phys. Rev. A **45**, 4911–4924 (1992).
2. S. Gangopadhyay, N. Melikechi, and E. E. Eyler, "Optical phase perturbations in nanosecond pulsed amplification and second-harmonic generation," J. Opt. Soc. Am. B **11**, 231–241 (1994).
3. N. Melikechi, S. Gangopadhyay, and E. E. Eyler, "Phase dynamics in nanosecond pulsed dye laser amplification," J. Opt. Soc. Am. B **11**, 2402–2411 (1994).
4. S. Gangopadhyay, "Optical phase distortions in nanosecond laser pulses and their effects on high-resolution spectroscopy," Ph.D. dissertation (U. of Delaware, 1995).
5. I. Reinhard, M. Gabrysch, B. Fischer von Weikersthal, K. Jungmann, and G. zu Pulitz, "Measurement and compensation of frequency chirping in pulsed dye laser amplifiers," Appl. Phys. B Photophys. Laser Chem. **63**, 467–472 (1996).
6. R. T. White, Y. He, B. J. Orr, M. Kono, and K. G. H. Baldwin, "Pulsed injection-seeded optical parametric oscillator with low frequency chirp for high-resolution spectroscopy," Opt. Lett. **28**, 1248–1250 (2003).
7. R. T. White, Y. He, B. J. Orr, M. Kono, and K. G. H. Baldwin, "Control of frequency chirp in nanosecond-pulsed laser spectroscopy. 1. Optical-heterodyne chirp analysis techniques," J. Opt. Soc. Am. B **21**, 1577–1585 (2004).
8. R. T. White, Y. He, B. J. Orr, M. Kono, and K. G. H. Baldwin, "Control of frequency chirp in nanosecond-pulsed laser spectroscopy. 2. A long-pulse optical parametric oscillator for narrow optical bandwidth," J. Opt. Soc. Am. B **21**, 1586–1594 (2004).
9. R. T. White, Y. He, B. J. Orr, M. Kono, and K. G. H. Baldwin, "Transition from single-mode to multimode operation of an injection-seeded pulsed optical parametric oscillator," Opt. Express **12**, 5655–5660 (2004).
10. M. Kono, K. G. H. Baldwin, Y. He, R. T. White, and B. J. Orr, "Heterodyne-assisted pulsed spectroscopy with a nearly Fourier-transform limited, injection-seeded optical parametric oscillator," Opt. Lett. **30**, 3413–3415 (2005).
11. K. S. E. Eikema, W. Ubachs, W. Vassen, and W. Hogervorst, "Precision measurements in helium at 58 nm: ground state Lamb shift and the $1\,^1S$–$2\,^1P$ transition isotope shift," Phys. Rev. Lett. **76**, 1216–1219 (1996).
12. K. S. E. Eikema, W. Ubachs, W. Vassen, and W. Hogervorst, "Lamb shift measurement in the $1\,^1S$ ground state of helium," Phys. Rev. A **55**, 1866–1884 (1996).
13. S. D. Bergeson, A. Balakrishnan, K. G. H. Baldwin, T. B. Lucatorto, J. P. Marangos, T. J. McIlrath, T. R. O'Brian, S. L. Rolston, C. J. Sansonetti, J. Wen, N. Westbrook, C. H. Cheng, and E. E. Eyler, "Measurement of the He ground state Lamb shift via the two-photon $1\,^1S$–$2\,^1S$ transition," Phys. Rev. Lett. **80**, 3475–3478 (1998).
14. S. D. Bergeson, A. Balakrishnan, K. G. H. Baldwin, T. B. Lucatorto, J. P. Marangos, T. J. McIlrath, T. R. O'Brian, S. L. Rolston, C. J. Sansonetti, J. Wen, C. H. Cheng, and E. E. Eyler, "Precision spectroscopy in He as a test of QED," Phys. Scr. **T83**, 76–82 (1999).
15. S. D. Bergeson, K. G. H. Baldwin, T. B. Lucatorto, T. J. McIlrath, C. H. Cheng, and E. E. Eyler, "Doppler-free two-photon spectroscopy in the vacuum ultraviolet: helium $1\,^1S$–$2\,^1S$ transition," J. Opt. Soc. Am. B **17**, 1599–1606 (2000).
16. C. Hagel, C. Nesi, L. Jozefowski, C. Schwob, F. Nez, and F. Biraben, "Accurate measurement of the frequency of the $6S$–$8S$ two-photon transitions in cesium," Opt. Commun. **160**, 1–4 (1999).
17. K. Sasaki, K. Sugiyama, V. Babychev, and A. Onae, "Two-photon spectroscopy of the $6S$–$8S$ transitions in cesium using an extended-cavity diode laser," Jpn. J. Appl. Phys. Part 1 **39**, 5310–5311 (2000).
18. R. T. White, "Quasi-phase-matched nonlinear-optical devices," Ph.D. thesis (Macquarie U., 2004).
19. J. Marek, "Radiative lifetime of the $8S$, $9S$ and $7D$ levels of

Cs I," Phys. Lett. **60A**, 190–192 (1977), and references therein.

20. D. S. Elliott, M. W. Hamilton, K. Arnett, and S. J. Smith, "Correlation effects of a phase diffusing field on two-photon absorption," Phys. Rev. A **32**, 887–895 (1985).

21. C. Chen, D. S. Elliott, and M. W. Hamilton, "Two-photon absorption from the real Gaussian field," Phys. Rev. Lett. **68**, 3531–3534 (1992).

22. B. Dayan, A. Pe'er, A. A. Friesem, and Y. Silberberg, "Two photon absorption and coherent control with broadband down-converted light," Phys. Rev. Lett. **93**, 023005, 1–4 (2004).